Hindawi Publishing Corporation
Journal of Nanomaterials
Volume 2016, Article ID 5940618, 7 pages
http://dx.doi.org/10.1155/2016/5940618

Research Article

Facile Synthesis of Electroconductive AZO@TiO_2 Whiskers and Their Application in Textiles

Hui Ma,[1,2] Qiang Gao,[1,2,3] Chunxia Gao,[3,4] Wei Bao,[5] and Mingqiao Ge[1,2]

[1]*Key Laboratory of Science and Technology of Eco-Textiles, Jiangnan University, Ministry of Education, Wuxi 214122, China*
[2]*College of Textile & Clothing, Jiangnan University, Wuxi 214122, China*
[3]*State Key Laboratory of Molecular Engineering of Polymers, Department of Macromolecular Science and Laboratory of Advanced Materials, Fudan University, Shanghai 200438, China*
[4]*Institute of Orthopaedics, The First Affiliated Hospital of Soochow University, Suzhou 215006, China*
[5]*Wuxi Entry-Exit Inspection and Quarantine Bureau, Wuxi 214101, China*

Correspondence should be addressed to Qiang Gao; gaoqiang@jiangnan.edu.cn and Chunxia Gao; cxgao@suda.edu.cn

Received 3 February 2016; Revised 2 August 2016; Accepted 3 August 2016

Academic Editor: Reza Bayati

The electroconductive AZO@TiO_2 whiskers have been successfully prepared *via* coating Al doped ZnO onto TiO_2 whisker. The orthogonal tests were employed to optimize the synthetic conditions. The crystallographic structure and the morphology of the AZO@TiO_2 whiskers and the polypropylene nonwoven fabrics modified with AZO@TiO_2 whiskers were characterized by X-ray photoelectron spectroscopy, X-ray diffraction, scanning electron microscope, four-probe meter, and electrometer. The results showed the AZO@TiO_2 whiskers exhibited good electroconductive performance. Moreover, the polypropylene nonwoven fabrics modified with AZO@TiO_2 whiskers revealed excellent antistatic performance indicating wide application of AZO@TiO_2 whiskers in the antistatic textiles.

1. Introduction

With the rapid development of nanotechnology, a great number of nanomaterials and nanostructures have been applied in diverse electronic and related fields. In recent years, many researchers have focused on the preparation of TiO_2 with different morphologies for special functional applications [1], such as nanotubes [2], nanorods [3–5], and nanowires [6]. Rod-like TiO_2 whiskers are more likely to disperse uniformly compared with nanoparticles, guaranteeing the good inner homogeneity [7]. Besides, the pathway for electron is readily formed as the rod materials overlap with each other, thus improving conductivity. However, the high electric resistance of TiO_2 limits its application. One effective approach to reduce the electric resistance is to dope electroconductive elements onto TiO_2 [8–10]. You et al. [11] prepared monodispersed Cu-doped TiO_2 nanorods with tunable lengths (2–30 nm), diameters (2–5 nm), and doping concentrations (1.7–3.2%) through a low temperature hydrolytic route. The surface-functionalized method was employed to synthesize TiO_2@CdS core-shell nanorods using citric acid as an agent by Das and De [12]. Nevertheless, the reported works only focus on the photoelectron chemical behavior; the conductivity of the TiO_2 whiskers coated with the conductive material has rarely been studied.

Al doped ZnO (AZO) is promising as a cost-effective replacement for other transparent conductors, such as In_2O_3: Sn (ITO), SnO_2: Sb (ATO), and SnO_2: F (FTO), due to its high thermal stability, low price, and nontoxicity characteristics [13, 14]. P-type doping of ZnO can be achieved *via* the addition of Al as the dopant [15]. AZO powders have been successfully prepared by a simple chemical coprecipitation method by Zhang et al. [16] and the photocatalytic and electrical properties were improved compared to those of ZnO. Wu et al. synthesized aluminum and gallium codoped ZnO powders (AGZ), which led to fine grain size ranging

from 14 to 28 nm and low resistivity of 2.518×10^3 Ω·cm [17]. The conductivity is caused by the replacement of Zn^{2+} with Al^{3+}, releasing excessive electrons into the conduction band.

In this study, the Al doped ZnO materials coatings onto TiO_2 whiskers were synthesized by a facile hydrothermal method. The microstructure, morphology, and electrical performance of the AZO@TiO_2 whiskers were investigated. The properties of the polypropylene nonwoven fabrics modified with the AZO@TiO_2 whiskers were further studied.

2. Experiment

2.1. Materials. TiO_2 nanoparticles with an average diameter of 250 ± 35 nm were purchased from Jianghu Chemical Industry Co., Ltd., China. $Al(NO)_3 \cdot 9H_2O$, $Zn(NO_3)_2 \cdot 6H_2O$, and NaOH were purchased from Sinopharm Chemical Reagent Co. Ltd., China. All the chemicals and reagents used in this study were of analytical grade.

2.2. Preparation of Electroconductive AZO@TiO_2 Whiskers

2.2.1. Preparation of TiO_2 Whiskers. The TiO_2 whiskers were prepared by two-step synthesis. Generally, TiO_2 nanoparticles and K_2CO_3 with the molar ratio of $n(\text{Ti})/n(K_2CO_3)$ = 4 were firstly mixed in distilled water. After dispersing in ultrasonic cleaner (100 W) for 30 min, the mixture was heated and blended with magnetic stirrer. When it became sticky, the dope was transferred into drying oven. After grinding process, the dried powders were performed in a muffle furnace at 1000°C for 10 h in order to form $K_2Ti_4O_9$ whisker bunches and then boiled for 8 h in deionized water to disperse into the sole whiskers. After the HCl (60 mol/L) treatment for 6 h in the thermostatic water bath, the precursor was annealed at 1000°C for 5 h with the speed of 5°/min to obtain TiO_2 whiskers.

2.2.2. Preparation of AZO@TiO_2 Whiskers. Firstly, $Zn(NO_3)_2 \cdot 6H_2O$ was dissolved in distilled water with an amount of $Al(NO)_3 \cdot 9H_2O$ further added into the $Zn(NO_3)_2$ solution to obtain the desired solution A. The suspension was made with TiO_2 nanoparticles and 100 mL distilled water. After the ultrasonic treatment for 30 min, it was poured into a three-necked flask. A mixed acid solution of A was added to the suspension drop by drop at 65°C with stirring (300 rpm). The pH value was maintained with the buffer solution during the process. After a 120 min reaction, the white precipitation was filtered and washed with distilled water and dried in a drying oven at 70°C. After the sintering, the electroconductive AZO@TiO_2 whiskers were obtained.

2.3. Preparation of Antistatic Fabric. After cleaning with detergents and washed with distilled water, all the polypropylene nonwoven fabrics (40 cm × 45 cm) were dried in the oven for 24 h. The synthesized size, consisting of sticking agent (Guangdong Gongchenrihua Co., Ltd., China) and thickening agent (Shenzhen Yongzhiqiang Chemical Technology Co., Ltd., China), was mixed with 0.1, 0.2, 0.3, 0.4, and 0.5 wt% electroconductive AZO@TiO_2 whiskers. The polypropylene nonwoven fabrics were prepared with the mixture by surface coating manually. After coating, the fabrics were dried in vacuum oven for 1 h.

2.4. Characterization. The TiO_2 whiskers were fabricated from TiO_2 and K_2CO_3 nanoparticles in a stable reactor, which could be heated up to 1000°C with a controllable heat rate of 10°/min by an automatic tube furnace (GSL 1600X, Hefei Kejing Materials Technology, China).

The morphology of the electroconductive AZO@TiO_2 whiskers was examined by scanning electron microscope (SEM) (SU-1510, Hitachi, Japan) operated at 10 kV. The samples were gold-sputtered on the surface to ensure the electrical conductivity and observed in vacuum environment to eliminate air impact. XRD analysis was performed using the X-ray powder diffraction (XRD) (D8 Advance, Bruker, Germany) with monochromated Cu-Kα radiation (λ = 1.54183 Å) across a 2θ range of 10–80° with a rate of 0.1 s/step. The component of electroconductive AZO@TiO_2 whiskers was conducted with the X-ray photoelectron spectroscopy (XPS) (ESCALAB 250Xi, Thermo Fisher Scientific, America), employing a soft X-ray source of Al-Kα ($h\nu$ = 1486.6 eV) and operating at 150 W.

The surface resistivity of the electroconductive AZO@TiO_2 whiskers was manifested by the four-probe meter (SZT-2A, Tongchuang Electronic, China). The antistatic property of nonwoven fabric was measured by fabric induced electrostatic measuring instrument (YG (B) 342D, Darong Textile Instrument, China).

3. Results and Discussion

3.1. Orthogonal Test for Electroconductive AZO@TiO_2 Whiskers. Orthogonal design is one of the most effective and time-saving methods for the studies involving multiple variables in order to find out which factors (or variables) influence to the most extent properties of the target product [18]. Besides, it provides a powerful way to find an optimal combination of a smaller number of arrays to obtain the optimum thus reducing more experiments associated with the analysis [19, 20]. Based on our previous experimental results, the main factors, including calcination temperature, pH, doping ratio (Al/Zn), and coating ratio (Zn/Ti), affected the formation process of electroconductive AZO@TiO_2 whiskers. In this study, the L_9 (2^3) orthogonal array of the Taguchi method [21] was adopted to investigate these factors and optimize the synthetic conditions. The factors and levels are listed in Table 1. Table 2 and Figure 1 present the experimental results of the L_9 (2^3) orthogonal array. The surface resistivity of resultant AZO@TiO_2 whiskers was measured. The surface resistivity at level I for factor A (B, C, or D) is as follows:

$$K_{iA(B,C,\text{ or }D)} = \frac{\sum_1^a (b, c \text{ or } d)}{nA\,(B, C \text{ or } D)}$$
$$R_{A(B,C \text{ or } D)} = \max\left\{K_{iA(B,C,\text{ or }D)}\right\} - \min\left\{K_{iA(B,C,\text{ or }D)}\right\}, \quad (1)$$

Table 1: Factors and levels of orthogonal design.

Levels	*A* Coating ratio/%	*B* Doping ratio/%	*C* pH	*D* Calcination temperature/°C
1	45	2	8	400
2	55	2.5	9	500
3	65	3	10	600

Symbols *A*, *B*, *C*, and *D* represent factors of coating ratio, doping ratio, pH, and calcination temperature. Symbols 1, 2, and 3 represent concentration levels of each factor.

Table 2: L_9 (2^3) orthogonal array and experimental results.

Trial number	*A* Coating ratio/at%	*B* Doping ratio/at%	*C* pH	*D* Calcination temperature/°C	Surface resistivity/(KΩ·cm)
	1	2	3	4	
1	1 (45)	1 (2)	3 (10)	2 (500)	26.9
2	2 (55)	1	1 (8)	1 (400)	8.7
3	3 (65)	1	2 (9)	3 (600)	21.7
4	1	2 (2.5)	2	1	4.3
5	2	2	3	3	31.6
6	3	2	1	2	5.0
7	1	3 (3)	1	3	26.7
8	2	3	2	2	39.7
9	3	3	3	1	41.3
K_1	19.3	19.1	13.5	18.1	—
K_2	26.6	13.6	21.9	23.9	—
K_3	22.7	35.9	33.3	26.7	—
R	7.4	22.3	19.8	8.6	—

The arrangements of columns *A*, *B*, *C*, and *D* were decided by orthogonal design for 4 (factor) ∗ 9 (run number); every row of run number represents one experimental replicate; every run was carried out twice.

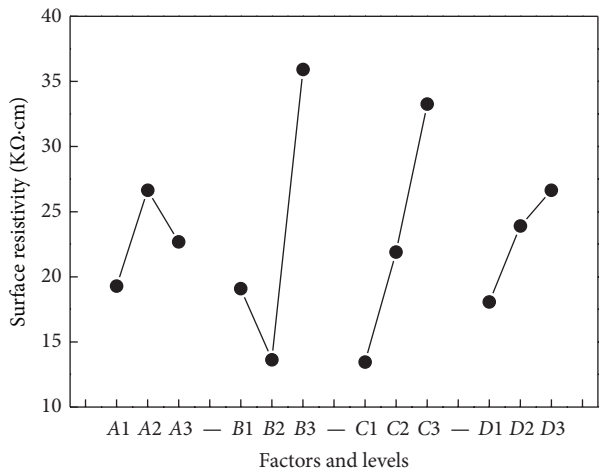

Figure 1: The trends between factors and levels and surface resistivity.

where *a*, *b*, *c*, and *d* represent the numbers of levels for factors *A*, *B*, *C*, and *D* and R_A, R_B, R_C, and R_D represent the ranges, which affect the influences of levels on the experimental result.

Table 3: Coating ratio and surface resistivity.

Coating ratio/at%	15	25	35	45
Surface resistivity/KΩ·cm	98.9	65.3	41.6	36.5

According to the value of *R* in Table 2, the influence of four factors on the electroconductivity of AZO@TiO_2 whisker decreases in the order: doping ratio > pH > calcinations temperature > coating ratio. Doping ratio and pH value are the dominant factors over others.

Our previous studies showed that the conductivity was enhanced with the increase of coating ratio (Sn/Ti) when TiO_2 nanoparticles were encapsulated by ATO [22]. In this study, we continue to optimize the doping ratio to find the lowest surface resistivity as shown in Table 3. The lowest surface resistivity was approached when the coating ratio was 45 at%. Nevertheless, when the coating ratio continues to increase, the electroconductivity was deteriorated, which indicates that the coating ratio has been saturated.

In the factor of doping ratio, the surface resistivity of AZO@TiO_2 whiskers decreases at first and then increases steadily at the optimal level of 2.5 at%. Al^{3+} is ready to substitute Zn^{2+} position to form negatively charged lattice

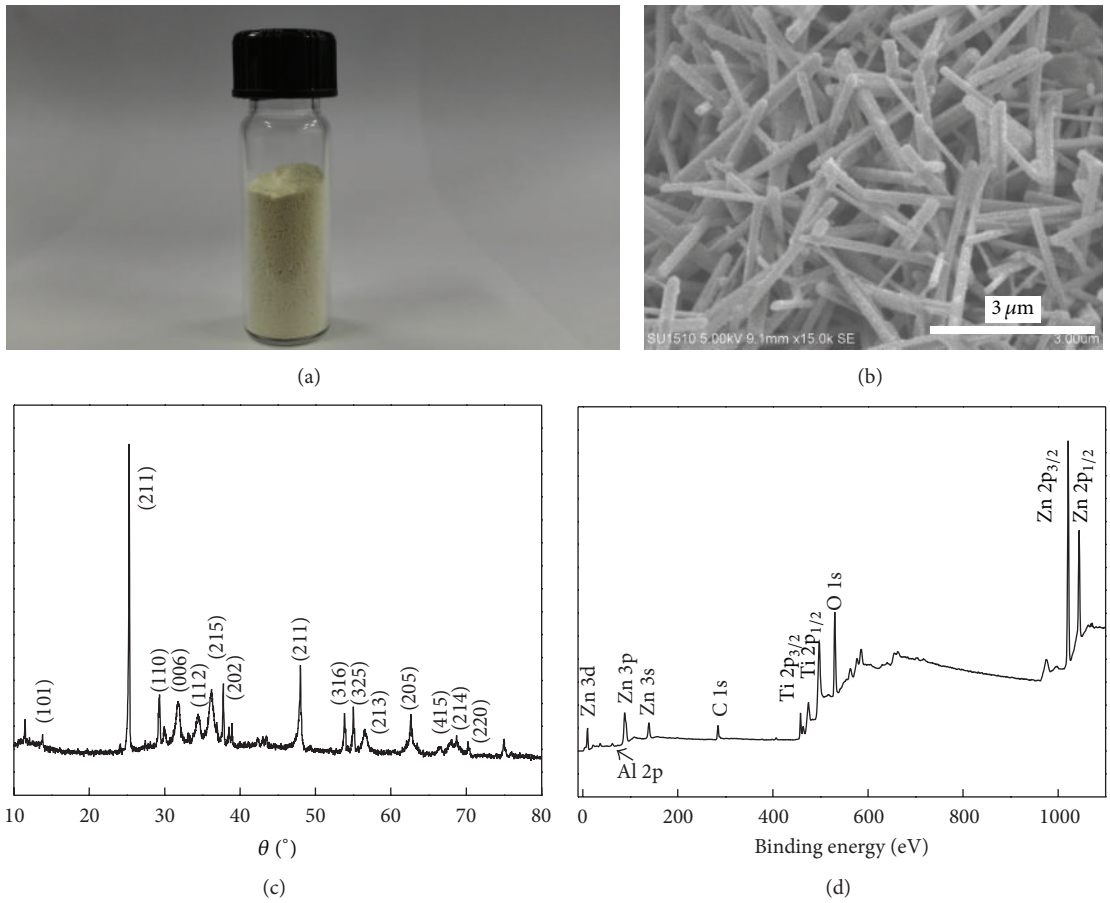

FIGURE 2: (a) The digital photo of AZO@TiO_2 whiskers; (b) SEM image of AZO@TiO_2 whiskers; (c) XRD pattern of AZO@TiO_2 whiskers; (d) XPS pattern of AZO@TiO_2 whiskers.

defects as the radius of Al^{3+} is smaller than Zn^{2+}. Therefore, a free electron emerges. The conductivity would increase with the implement of Al^{3+} contents when doping ratio is below 2.5 at%. The excess Al would form $ZnAl_2O_3$ rather than replace Zn^{2+} lattice site, which increases the resistivity. According to the report of Chen et al. [23] and Lu et al. [24], $ZnAl_2O_4$ would lead to the increasing resistivity of AZO.

The pH value also has a big impact on the conductivity of AZO@TiO_2 whiskers, as it offers the opportunities for the suitable reactive environment. According to reaction equation (2), $Zn(OH)_4{}^{2-}$ is prepared in alkaline conditions and uniformly coated on the surface of TiO_2 whiskers. With further dehydration reaction, the H_2O is removed as shown in reaction equation (3):

$$Zn^{2+} + 2OH^- + 2H_2O \longrightarrow Zn(OH)_4{}^{2-} + 2H^+ \quad (2)$$

$$OH^- + OH^- \longrightarrow H_2O + O_2{}^- \quad (3)$$

The influences of calcination temperature and coating ratio are relatively small that the resistivity fluctuated between 18 KΩ·cm and 26 KΩ·cm. The optimal condition of resistivity was as follows: doping ratio = 2.5 at%, pH = 8, calcination temperature = 400°C, and coating ratio = 45 at%. Due to the fact that the optimal experiment is out of nine groups in Table 2, we carried out another experiment according to the optimal condition and minimal surface resistivity of 3.6 KΩ·cm was approached.

3.2. Properties of Electroconductive AZO@TiO_2 Whiskers. The electroconductive AZO@TiO_2 whiskers are yellow in color and small in size, as revealed in Figure 2(a). Figure 2(b) shows the SEM image of AZO@TiO_2 whiskers. AZO@TiO_2 whiskers are rod-like, with a diameter of 280–340 nm and a length of 1.95–3.75 μm. Furthermore, coating layer of AZO locates on the surface of TiO_2 whiskers, where the electrons could be freely spread among whiskers when they are connected with each other and readily conduct electricity within the materials.

Figure 2(c) reveals the XRD pattern of synthetic whiskers. The characteristic peaks of rutile TiO_2 (JCPDS no. 65-5714) can be clearly observed from the XRD pattern of AZO@TiO_2 whiskers [25]. Meanwhile, hexagonal wurtzite zincite peaks [26] (namely, 2θ = 28.3°, 31.4°, 47.7°) were also observed, indicating that the AZO has been deposited onto the TiO_2 whisker.

XPS analysis was employed to further confirm the chemical composition of the synthetic whiskers. Figure 2(d) illustrates that synthetic whiskers consist of Zn, C1s, O,

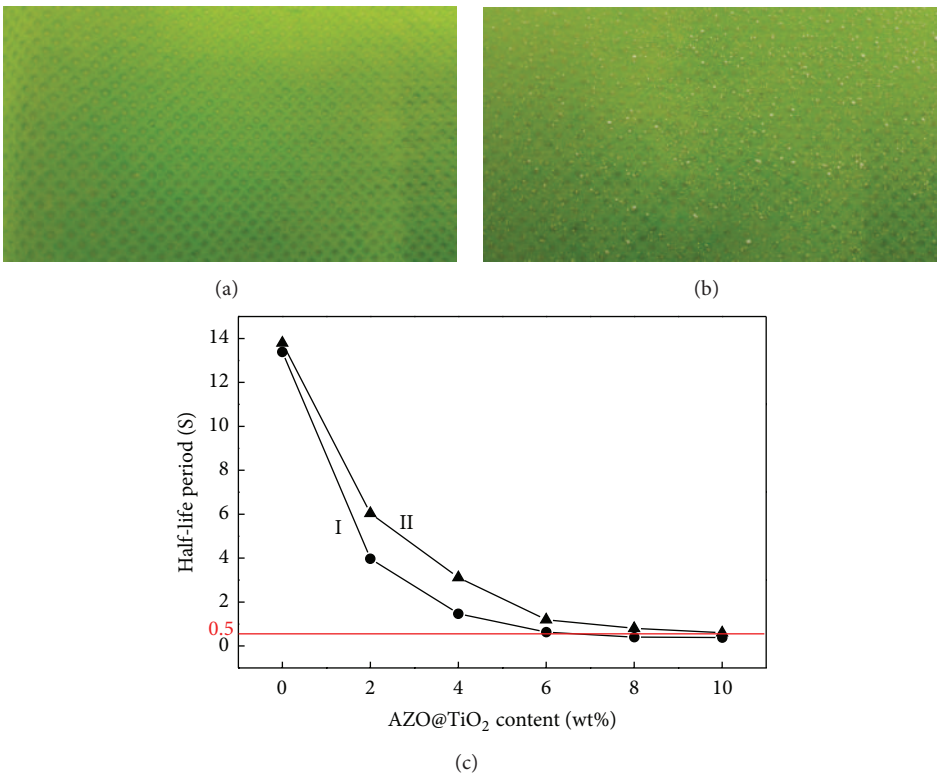

Figure 3: (a) Pure polypropylene nonwoven fabrics; (b) polypropylene nonwoven fabrics coated with AZO@TiO_2 whiskers; (c) the relationship between the content of AZO@TiO_2 whiskers and fading period of half-life voltage before washing (I) and after washing for 20 times (II).

and Ti elements. Among them, the binding energy of C 1s peak was at 284.8 eV and used as the reference standard. With scanning over the corresponding XPS spectra area, the binding energies for the Zn 2p region at around 1000 eV were analyzed. The peak located at 1044.43 eV was the same as Zn $2p_{3/2}$ and the other one located at 1021.53 eV was assigned to Zn $2p_{1/2}$, while those of Zn 3d, Zn 3p, and Zn 3s were located at 10.08 eV, 88.08 eV, and 139.08 eV, respectively. These peak positions agree with the reference values, suggesting a normal state of AZO in AZO@TiO_2 whisker [27, 28]. The binding energy of O 1s peak was at 530.08 eV, clarifying the existence of TiO_2 whisker. The Ti $2p_{3/2}$ and Ti $2p_{1/2}$ peaks also had obvious double peaks at binding energies of 458.53 eV and 475.33 eV, respectively, indicting a normal state of TiO_2 in AZO@TiO_2 whisker [5].

3.3. Antistatic Fabric Coated with AZO@TiO_2 Whiskers. The coating method is of special interest in fabrication of nanostructured materials such as nanocomposite coatings carrying a variety of functionalities [29]. A layer of electroconductive AZO@TiO_2 whiskers was coated on the surface of polypropylene nonwoven fabrics. Compared with the uncoated polypropylene nonwoven fabrics in Figure 3(a), the electroconductive AZO@TiO_2 whiskers were coated onto the surface (Figure 3(b)). The influence of the content of AZO@TiO_2 whiskers on the antistatic property of fabrics was shown in Figure 3(c)I. With increased AZO@TiO_2 whiskers, the half-life voltage of fabrics decreased sharply at first. When the content is more than 4 wt%, the tendency to decrease is slow, and the half-life voltage drops to 1.47 s. This suggests that the modified fabrics have good antistatic property. When the content is 8 wt%, the half-life voltage is 0.401 s (<0.5), which indicates that the coated fabrics reach the index of excellent antistatic property (the red line). Meanwhile, antistatic property after washing is very important for surface-modified fabrics. If it is poor, the antistatic property does not remain for long [30]. Changes in the half-life voltage with different amount of AZO@TiO_2 whiskers after washing for 20 times are shown in Figure 3(c)II, similar to Figure 3(c)I. In addition, when the content of AZO@TiO_2 whiskers reached 10 wt%, the half-life voltage of surface-modified fabrics after washing for 20 times was 0.481 s (<0.5) still meeting the requirement of excellent antistatic property.

The application of fiber materials is limited in some particular environment due to the high resistance. The electroconductive AZO@TiO_2 whiskers with unique rod-shaped structure and excellent conductivity own a wide future application in the functional textiles.

4. Conclusion

In summary, the rod-like electroconductive AZO@TiO_2 whiskers were successfully fabricated by coating Al doped ZnO onto TiO_2 whiskers. The optimal synthetic condition

for electroconductive AZO@TiO_2 whiskers was obtained with doping ratio of 2.5 at%, pH value of 8, calcination temperature of 400°C, and coating ratio of 45 at%. The electroconductive AZO@TiO_2 whiskers are light yellow with a length to diameter ratio of 5.6. The polypropylene nonwoven fabrics modified with AZO@TiO_2 whiskers exhibited excellent antistatic performance and laundering durability, indicating wide application of AZO@TiO_2 whiskers in the antistatic textiles.

Competing Interests

The authors declare that they have no competing interests.

Acknowledgments

The authors acknowledge financial support from Natural Science Foundation of China (Grant no. 21504033), China Postdoctoral Science Foundation (Grant no. 2015M580296), State Key Laboratory of Molecular Engineering of Polymers (Fudan University) (Grant no. K2016-04), Fundamental Research Funds for the Central Universities of China (no. JUSRP11444), the Research Project of Jiangsu Entry-Exit Inspection and Quarantine Bureau (Grant no. 2015KJ18), Jiangsu Province Key Laboratory of Silk Engineering (Grant no. KJS1413) and Open Project Program of Key Laboratory of Eco-Textiles, Jiangnan University, Ministry of Education (Grant no. KLET1403), Fundamental Research Funds for Graduate Education Innovation Project of Jiangsu Province in 2015 (no. SJZZ15_0146), and a project funded by the Priority Academic Program Development of Jiangsu Higher Education Institutions.

References

[1] T. Leshuk, R. Parviz, P. Everett, H. Krishnakumar, R. A. Varin, and F. Gu, "Photocatalytic activity of hydrogenated TiO_2," *ACS Applied Materials & Interfaces*, vol. 5, no. 6, pp. 1892–1895, 2013.

[2] P. Roy, S. Berger, and P. Schmuki, "TiO_2 nanotubes: synthesis and applications," *Angewandte Chemie—International Edition*, vol. 50, no. 13, pp. 2904–2939, 2011.

[3] I. S. Cho, Z. Chen, A. J. Forman et al., "Branched TiO_2 nanorods for photoelectrochemical hydrogen production," *Nano Letters*, vol. 11, no. 11, pp. 4978–4984, 2011.

[4] T. A. Kandiel, R. Dillert, A. Feldhoff, and D. W. Bahnemann, "Direct synthesis of photocatalytically active rutile TiO_2 nanorods partly decorated with anatase nanoparticles," *Journal of Physical Chemistry C*, vol. 114, no. 11, pp. 4909–4915, 2010.

[5] J.-N. Nian and H. Teng, "Hydrothermal synthesis of single-crystalline anatase TiO_2 nanorods with nanotubes as the precursor," *The Journal of Physical Chemistry B*, vol. 110, no. 9, pp. 4193–4198, 2006.

[6] H.-W. Shim, D. K. Lee, I.-S. Cho, K. S. Hong, and D.-W. Kim, "Facile hydrothermal synthesis of porous TiO_2 nanowire electrodes with high-rate capability for Li ion batteries," *Nanotechnology*, vol. 21, no. 25, Article ID 255706, 2010.

[7] H. Zhu, T. Jie, and D. Xiang, "Preparation and photoelectrochemical activity of Cr-doped TiO_2 nanorods with nanocavities," *The Journal of Physical Chemistry C*, vol. 114, no. 7, pp. 2873–2879, 2010.

[8] S. Park, S.-D. Seo, S. Lee et al., "Sb:SnO_2@TiO_2 heteroepitaxial branched nanoarchitectures for Li ion battery electrodes," *The Journal of Physical Chemistry C*, vol. 116, no. 41, pp. 21717–21726, 2012.

[9] M. Xu, P. Da, H. Wu, D. Zhao, and G. Zheng, "Controlled Sn-doping in TiO_2 nanowire photoanodes with enhanced photoelectrochemical conversion," *Nano Letters*, vol. 12, no. 3, pp. 1503–1508, 2012.

[10] Q. Liu, L. Zhang, J.-F. Chen, and Y. Le, "Synthesis of TiO_2@ATO core–shell nanofibers using coaxial electrospinning," *Materials Letters*, vol. 137, pp. 339–342, 2014.

[11] M. You, T. G. Kim, and Y.-M. Sung, "Synthesis of Cu-doped TiO_2 nanorods with various aspect ratios and dopant concentrations," *Crystal Growth and Design*, vol. 10, no. 2, pp. 983–987, 2009.

[12] K. Das and S. K. De, "Optical properties of the type-II core-shell TiO_2@CdS nanorods for photovoltaic applications," *The Journal of Physical Chemistry C*, vol. 113, no. 9, pp. 3494–3501, 2009.

[13] S. Vunnam, K. Ankireddy, J. Kellar, and W. Cross, "Environmental stability of solution processed Al-doped ZnO naoparticulate thin films using surface modification technique," *Applied Surface Science*, vol. 322, pp. 1–5, 2014.

[14] Y.-S. Luo, J.-P. Yang, X.-J. Dai, Y. Yang, and S.-Y. Fu, "Preparation and optical properties of novel transparent al-doped-ZnO/epoxy nanocomposites," *The Journal of Physical Chemistry C*, vol. 113, no. 21, pp. 9406–9411, 2009.

[15] Q. X. Xia, K. S. Hui, K. N. Hui et al., "High quality p-type N-doped AZO nanorod arrays by an ammonia-assisted hydrothermal method," *Materials Letters*, vol. 78, pp. 180–183, 2012.

[16] P. Zhang, R. Y. Hong, Q. Chen, and W. G. Feng, "On the electrical conductivity and photocatalytic activity of aluminum-doped zinc oxide," *Powder Technology*, vol. 253, pp. 360–367, 2014.

[17] R. Wu, W. Zhang, H. Zhang et al., "Investigation of aluminum and gallium co-doped ZnO powders and their effects on the properties of targets," *Materials Science in Semiconductor Processing*, vol. 19, no. 1, pp. 24–31, 2014.

[18] M. Dargahi, H. Kazemian, M. Soltanieh, M. Hosseinpour, and S. Rohani, "High temperature synthesis of SAPO-34: applying an L9 Taguchi orthogonal design to investigate the effects of experimental parameters," *Powder Technology*, vol. 217, pp. 223–230, 2012.

[19] S. Ma, H. Wang, Y. Wang, H. Bu, and J. Bai, "Bio-hydrogen production from cornstalk wastes by orthogonal design method," *Renewable Energy*, vol. 36, no. 2, pp. 709–713, 2011.

[20] S.-Q. Liu, C.-F. Dai, L. Wang, S.-P. Li, and X.-D. Li, "Orthogonal test design for optimization of synthesis of MTX/LDHs hybrids by ion-exchange method," *Journal of Physics and Chemistry of Solids*, vol. 79, pp. 82–88, 2015.

[21] M. Olivia and H. Nikraz, "Properties of fly ash geopolymer concrete designed by Taguchi method," *Materials and Design*, vol. 36, pp. 191–198, 2012.

[22] Q. Gao, H. Ma, W. Bao, C. Gao, and M. Ge, "Polyacrylonitrile/electroconductive TiO_2 nanoparticles composite fibers via wet-spinning," *Fibers and Polymers*, vol. 17, no. 7, pp. 1048–1054, 2016.

[23] Z. Chen, G. Zhan, Y. Wu, X. He, and Z. Lu, "Sol-gel-hydrothermal synthesis and conductive properties of Al-doped ZnO nanopowders with controllable morphology," *Journal of Alloys and Compounds*, vol. 587, pp. 692–697, 2014.

[24] Z. Lu, J. Zhou, A. Wang, N. Wang, and X. Yang, "Synthesis of aluminium-doped ZnO nanocrystals with controllable morphology and enhanced electrical conductivity," *Journal of Materials Chemistry*, vol. 21, no. 12, pp. 4161–4167, 2011.

[25] M. Osada, M. Kobayashi, and M. Kakihana, "Enhanced dielectric response induced by controlled morphology in rutile TiO_2 nanocrystals," *Journal of the Ceramic Society of Japan*, vol. 121, no. 1416, pp. 593–597, 2013.

[26] Y. Zhang, Y. Yang, J. Zhao et al., "Optical and electrical properties of aluminum-doped zinc oxide nanoparticles," *Journal of Materials Science*, vol. 46, no. 3, pp. 774–780, 2011.

[27] X. Q. Wei, B. Y. Man, M. Liu, C. S. Xue, H. Z. Zhuang, and C. Yang, "Blue luminescent centers and microstructural evaluation by XPS and Raman in ZnO thin films annealed in vacuum, N_2 and O_2," *Physica B: Condensed Matter*, vol. 388, no. 1-2, pp. 145–152, 2007.

[28] X. Tian, Z. Pan, H. Zhang et al., "Growth and characterization of the Al-doped and Al–Sn co-doped ZnO nanostructures," *Ceramics International*, vol. 39, no. 6, pp. 6497–6502, 2013.

[29] M. Jafari, A. Rahimi, P. Shokrolahi, and A. E. Langroudi, "Synthesis of antistatic hybrid nanocomposite coatings using surface modified indium tin oxide (ITO) nanoparticles," *Journal of Coatings Technology Research*, vol. 11, no. 4, pp. 587–593, 2014.

[30] D. Wang, Y. Lin, Y. Zhao, and L. Gu, "Polyacrylonitrile fibers modified by nano-antimony-doped tin oxide particles," *Textile Research Journal*, vol. 74, no. 12, pp. 1060–1065, 2004.